



저작자표시-비영리-변경금지 2.0 대한민국

이용자는 아래의 조건을 따르는 경우에 한하여 자유롭게

- 이 저작물을 복제, 배포, 전송, 전시, 공연 및 방송할 수 있습니다.

다음과 같은 조건을 따라야 합니다:



저작자표시. 귀하는 원저작자를 표시하여야 합니다.



비영리. 귀하는 이 저작물을 영리 목적으로 이용할 수 없습니다.



변경금지. 귀하는 이 저작물을 개작, 변형 또는 가공할 수 없습니다.

- 귀하는, 이 저작물의 재이용이나 배포의 경우, 이 저작물에 적용된 이용허락조건을 명확하게 나타내어야 합니다.
- 저작권자로부터 별도의 허가를 받으면 이러한 조건들은 적용되지 않습니다.

저작권법에 따른 이용자의 권리는 위의 내용에 의하여 영향을 받지 않습니다.

이것은 [이용허락규약\(Legal Code\)](#)을 이해하기 쉽게 요약한 것입니다.

[Disclaimer](#)

2014年
2月

2014年 2月
碩士學位 論文

碩士學位論文

Hydroxyapatite Coating on
Nanotubular Ti-25Ta-xZr
Alloys by RF-Sputtering
after Electrochemical
Deposition for Biomaterials

Hydroxyapatite Coating on Nanotubular Ti-25Ta-xZr Alloys
by RF-Sputtering after Electrochemical Deposition for Biomaterials

朝鮮大學校 大學院

光技術工學科(光應用工學專攻)

金
炫
柱

金 炫 柱

Hydroxyapatite Coating on Nanotubular Ti-25Ta-xZr Alloys by RF-Sputtering after Electrochemical Deposition for Biomaterials

나노튜브 형성된 Ti-25Ta-xZr 합금에 전기화학적인 석출 후,
RF-Sputtering을 이용한 HA 코팅

2014年 2月 25日

朝鮮大學校 大學院

光技術工學科(光應用工學專攻)

金 炫 柱

Hydroxyapatite Coating on
Nanotubular Ti-25Ta-xZr
Alloys by RF-Sputtering
after Electrochemical
Deposition for Biomaterials

指導教授 崔 漢 喆

이 論文을 工學 碩士學位申請 論文으로 提出함

2013年 10月

朝鮮大學校 大學院

光技術工學科(光應用工學專攻)

金 炫 柱

金炫柱의 碩士學位論文을 認准함

委員 張 朝鮮大學校 教授 金炳勳 印

委員 朝鮮大學校 教授 安相建 印

委員 朝鮮大學校 教授 崔漢喆 印

2013年 11月

朝鮮大學校 大學院

CONTENTS

LIST OF TABLES	III
LIST OF FIGURES	IV
국문초록	VI
I . INTRODUCTION	1
II . BACKGROUND	3
2.1. Titanium and titanium alloys	3
2.1.1 Alpha titanium alloys	3
2.1.2 Beta titanium alloys	4
2.1.3 Alpha + beta titanium alloys	4
2.2. Anodization	7
2.2.1 Nanotube formation on the Ti alloy	9
2.3. Hydroxyapatite (HA)	13
2.4. Surface treatment method for HA coating	15
2.4.1 Electrochemical deposition of HA	18
2.4.2 The sputtering process for HA coating	19
III . MATERIALS AND METHODS	21
3.1. Preparation of Ti-25Ta-xZr alloys	21
3.2. Analysis of surface characteristics for Ti-25Ta-xZr alloys	21
3.3. Nanotubular oxide formation on the alloy surface.....	23
3.4. HA coating on nanotubular Ti-25Ta-xZr alloys by electrochemical deposition method	24
3.5. HA coating by the radio-frequency(RF) magnetron sputtering	27
3.6. Surface wettability test	29
IV . RESULTS AND DISCUSSION	30
4.1. Microstructures of Ti-25Ta-xZr alloys	30

4.2. The nanotubular structure of Ti-25Ta-xZr alloy	35
4.3. The HA coating on nanotubular Ti-25Ta-xZr alloys by electrochemical deposition method	38
4.4. The RF-sputtered HA coating on HA deposited Ti-25Ta-xZr alloys	45
4.5. Wettability of Ti-25Ta-xZr alloys with various surface modification	48
V. CONCLUSIONS	50
- REFERENCES -	52

LIST OF TABLES

Table 1. Alloying elements of titanium and their effect.....	6
Table 2. Comparision of TiO ₂ nanotube fabrication methods.....	8
Table 3. The calcium phosphate phases used to date for coatings in orthopaedic devices	14
Table 4. Different technique to deposit HA coatings	17
Table 5. Electrochemical HA precipitation condition	25
Table 6. The coating condition of RF sputtering	28
Table 7. Volume ratio of pores and pore wall surface areas on nanotube layers	43

LIST OF FIGURES

Fig. 1. The phase diagram of titanium as a function of temperature and pressure shows martensitic transformations between the α , β and ω phases	5
Fig. 2. Anodic growth of the oxide film	11
Fig. 3. Schematic diagram of the evolution of a nanotube array at constant anodization voltage	12
Fig. 4. History of surface treatment technique to improve hard tissue compatibility	16
Fig. 5. Schematic diagram of the sputter system	20
Fig. 6. Process of monitoring voltage versus times during electrochemical HA deposition	26
Fig. 7. OM images of Ti-25Ta-xZr alloys after heat treatment at 1000 °C for 12 h in Ar atmosphere, followed by 0 °C water quenching	32
Fig. 8. FE-SEM images of Ti-25Ta-xZr alloys after heat treatment at 1000 °C for 12 h in Ar atmosphere, followed by 0 °C water quenching.....	33
Fig. 9. XRD peaks of Ti-25Ta-xZr alloys after heat treatment at 1000 °C for 12 h in Ar atmosphere, followed by 0 °C water quenching	34
Fig. 10. FE-SEM images of top, bottom, and cross-section for TiO ₂ nanotubes formed on Ti-25Ta-xZr alloys	37
Fig. 11. FE-SEM top view images of the HA coated film on nanotubular Ti-25Ta-xZr alloys by electrochemical deposition	39
Fig. 12. FE-SEM images and EDX analyses of the HA coated film on nanotubular Ti-25Ta-xZr alloys by electrochemical deposition	40
Fig. 13. FE-SEM images of pores and pore wall surface areas on nanotube layers.....	42
Fig. 14. Schematic diagram of the HA coated film on nanotubular Ti-25Ta-xZr alloys	44

Fig. 15. FE-SEM top view images of the RF-sputtered HA coating on HA deposited Ti-25Ta-xZr alloys 46

Fig. 16. FE-SEM images and EDX analyses of the RF-sputtered HA coating on HA deposited Ti-25Ta-xZr alloys 47

Fig. 17. Contact angle and snap shot of wettability on the surfaces 49

국 문 초 록

나노튜브 형성된 Ti-25Ta-xZr 합금에 전기화학적인 석출 후, RF-Sputteing을 이용한 HA 코팅

김 현 주

지도교수: 최한철, 공학/치의학박사

광응용공학과

조선대학교 대학원

티타늄 및 티타늄 합금은 좋은 기계적 특성 및 부식저항성, 우수한 생체적합성 때문에 생체재료로써 널리 사용되어 왔다. Ti-25Ta-xZr 삼원계 합금은 현재 사용되고 있는 Ti-6Al-4V 합금의 독성문제를 해결해줄 무독성원소로 이루어져 있으며, Zr 함량을 0, 3, 7 및 15 wt. % 가 되도록 변수를 주었으며, 아크멜팅법을 이용하여 합금을 설계하였다. 제조된 합금은 1000 °C에서 12시간동안 열처리한 후 급냉하여 두께 2.5 mm, 지름 10 mm의 디스크형태로 시편을 준비하였다. 1 M H₃PO₄ + 0.8 wt. % NaF를 첨가한 전해질 용액에서 양극산화 처리하여 표면에 나노튜브를 형성하였으며, 전기화학적인 방법과 물리적인 방법을 이용하여 거칠기를 부여한 표면에 하이드록시아파타이트 코팅을 하였다. 본 논문에서는, 양극산화법과 두 단계의 HA 코팅 법을 이용하여 합금표면에 나노구조의 거칠기를 부여하고 하이드록시아파타이트 코팅을 함으로써 뼈와의 접착성을 극대화시키는 연구를 진행하였다.

모든 시편의 표면특성은 OM, FE-SEM, EDS 및 XRD를 사용하여 분석하였다. 시편에 나노튜브를 형성 후, 하이드록시아파타이트를 코팅한 Ti-25Ta-xZr 합금 표면의 접촉각을 측정하여 표면 젖음성 (wettability)을 평가하여 다음과 같은 결과를 얻었다.

1. 광학현미경 분석 결과, Ti-25Ta 합금의 미세조직은 주로 마르텐사이트 구조가 관찰되었으나, Zr 함량이 증가할수록 마르텐사이트 구조가 사라지고 등축정 구조가 나타났다. 또한 XRD분석 결과 Ti-25Ta 합금에서 주로 α'' 피크를 보였으며

- Zr 함량이 증가할수록 α'' 의 피크가 감소하고, β 상의 피크가 증가하였다.
2. Zr 함량이 적은 합금의 경우는 나노튜브 배열이 불규칙하게 배열되었지만, Ti-25Ta-15Zr의 경우 큰 튜브 주위에 작은 튜브가 균일하게 배열되었다.
 3. Zr의 함량이 증가할수록, 나노튜브의 길이가 증가되었다.
 4. 전기화학적 증착법을 이용한 하이드록시아파타이트 코팅의 표면은 Ti-25Ta-3Zr까지는 나뭇잎 모양의 석출물 형태를 보였으며, Zr 함량이 증가할수록 꽃모양의 석출물 형태로 표면이 변화 하였다.
 5. 전기화학적인 방법으로 하이드록시아파타이트를 코팅한 후에, 물리적인 방법으로 HA를 코팅한 경우가 좀 더 조밀하고, 균일한 표면을 보였다. 코팅 표면의 조성분석은 EDS 분석 결과, 하이드록시아파타이트가 균일하게 형성되었다.
 6. 접촉각 측정결과, 나노튜브를 형성 후, 하이드록시아파타이트 코팅한 시편의 표면이 가장 낮은 접촉각을 보였다.

결론적으로, 나노튜브를 형성한 후 두 단계의 하이드록시아파타이트 코팅 처리한 Ti-25Ta-xZr 합금은 나노 구조를 형성하여 넓은 비표면적을 갖기 때문에 세포가 잘 자랄 수 있는 환경을 제공하였으며, 뼈와 유사한 성분인 하이드록시아파타이트를 코팅함으로써 골융합성을 향상시킬 수 있을 것으로 생각된다.

I . INTRODUCTION

Commercially pure titanium (Cp-Ti) and its alloys are the most common used as a dental implant material because of their good mechanical property, corrosion resistance and biocompatibility [1]. And Ti-6Al-4V alloy remained for some decades the implant materials. However, the Ti-6Al-4V alloy may cause serious health problems because of toxic metal ions [2]. For improving this problem, other Ti alloys with nontoxic elements such as Ta, Zr, Nb and Hf have been considered [3]. Ta is one of the most effective Ti β -stabilizer [4]. Moreover, Ta is found to reduce the modulus of elasticity when alloyed with Ti [5]. Also, the addition of Zr to Ti alloy results in high level of blood compatibility when used in cardiovascular implants and leads to better corrosion resistance due to the formation of stable ZrO_2 [6]. Therefore, the excellent characteristics of Ta and Zr have potential for dental Ti-Ta-Zr alloys due to their excellent mechanical properties, corrosion resistance and biocompatibility.

In the dental implant fields, the surface modification is very important for biocompatibility [7]. However, when Ti or Ti alloy is implanted in bone, the bonding of the implant with living bone frequently does not research. For improvement of biocompatibility of Ti alloy, we need the two scale surface modification. The nanotular surface with nano-scale on the native oxide will result in very strong reinforcement of the bone response [8]. It should be possible to control the nanotube size and morphology for biomedical implant use by controlling the applied voltage, alloying element, current density, anodization time, and electrolyte [9].

Also, hydroxyapatite [$Ca_{10}(PO_4)_6(OH)_2$, HA] coating on Ti or its alloys is important to improve the cell adhesion and proliferation [10]. HA is a biomaterial with calcium to phosphorus ratio resembles human bone. It has been used as a bone replacement material in restorative dental and orthopedic implants, and HA can improve bonding strength between body

tissues and an implant surface [11]. Electrochemical deposition of hydroxyapatite coating on Ti surface has unique advantages [12–15], which is an attractive process because highly complex objects can be coated relatively quickly at low process temperatures. Also, the thickness and chemical composition of coating can be well controlled through adequate conditions of the electrochemical deposition process [16]. The coating morphology can be controlled in the process of electrochemical deposition through the control of the deposition rate by varying the electrochemical potential, current density, electrolyte concentration and temperature [15, 17]. Also, radio frequency (RF) magnetron sputtering is a versatile deposition technique that can produce uniform, dense and hard coatings with a thickness $< 1 \mu\text{m}$ that are homogeneous in structure and composition [18]. Even though electro-deposited and RF-sputtered surface have many advantages, comparison of surface characteristics between electro-deposited and RF-sputtered surface was not researched. HA coated nanotubular surface can improve bone strength, reduce interfacial failure [16].

Therefore, in this study, we investigated hydroxyapatite coating on nanotubular Ti-25Ta-xZr alloys by RF-Sputtering after electrochemical deposition for biomaterials.

II . BACKGROUND

2.1. Titanium and titanium alloys [19]

Titanium (Ti) and its alloys are widely used in dental implants. Alloys such as Ti-6Al-4V and Ti-6Al-7Nb have good mechanical properties and are used in various orthopedic surgery and osteosynthesis systems such as parts of hip and knee implants, bone screws or plates. Ti system is useful for implant materials due to their high corrosion resistance as compared to stainless steel and Co-Cr-Mo alloys. Also, stable oxide TiO_2 film protects the surface of titanium and its alloys. This stable passive oxide film protects Ti alloys from pitting corrosion, intergranular corrosion, and crevice corrosion attack and in large part have qualification for the excellent biocompatibility of Ti alloys. Many of the alloys contain a mixture of α and β phases, whose morphologies and distributions can be transferred by processing or heat treatment. In addition, depending on alloy composition, the metastable β phase can decompose on cooling to mixtures of α and β , martensite or a metastable transition phase. Alloying additions also can influence the microstructures and properties. Table 1 shows the details of alloying elements added to titanium and their effect in stabilizing the various phases.

2.1.1 Alpha titanium alloys [20]

α -Ti alloys maintain their hcp crystallographic structures at room temperature and contain elements such as aluminium and tin. These α -stabilizing elements increase the phase transformation temperature. They exhibit good strength, toughness and corrosion resistance but poorer forgeability than β -alloys. α -alloys are used in suitable cryogenic applications since hcp phase materials do not exhibit ductile-brittle

transformation.

2.1.2 Beta titanium alloys [21]

β -Ti alloys contain elements such as vanadium, molybdenum, niobium and tantalum, which decrease the temperature of the α to β phase transition. Beta alloys are also prone to ductile-brittle transformation, therefore β -Ti alloys are easily cold form-able. But the major alloying elements for β -alloys are considered to be very biocompatible, more so than the α -stabilizing elements like aluminum and tin. The β -alloys also offer the unique characteristic of low elastic modulus and superior corrosion resistance.

2.1.3 Alpha-beta titanium alloys [22]

$\alpha + \beta$ alloys contain the metallurgically balanced amounts of both α and β stabilizers. The properties of these alloys can be controlled through heat treatment, which is used to adjust the amounts and types of phases present. $\alpha + \beta$ alloys generally have good fabricability as well as high tensile strength versus fracture toughness, good creep resistance versus low cycle fatigue, high tensile strength versus high cycle fatigue. The most commonly used $\alpha + \beta$ alloy is Ti-6Al-4V.

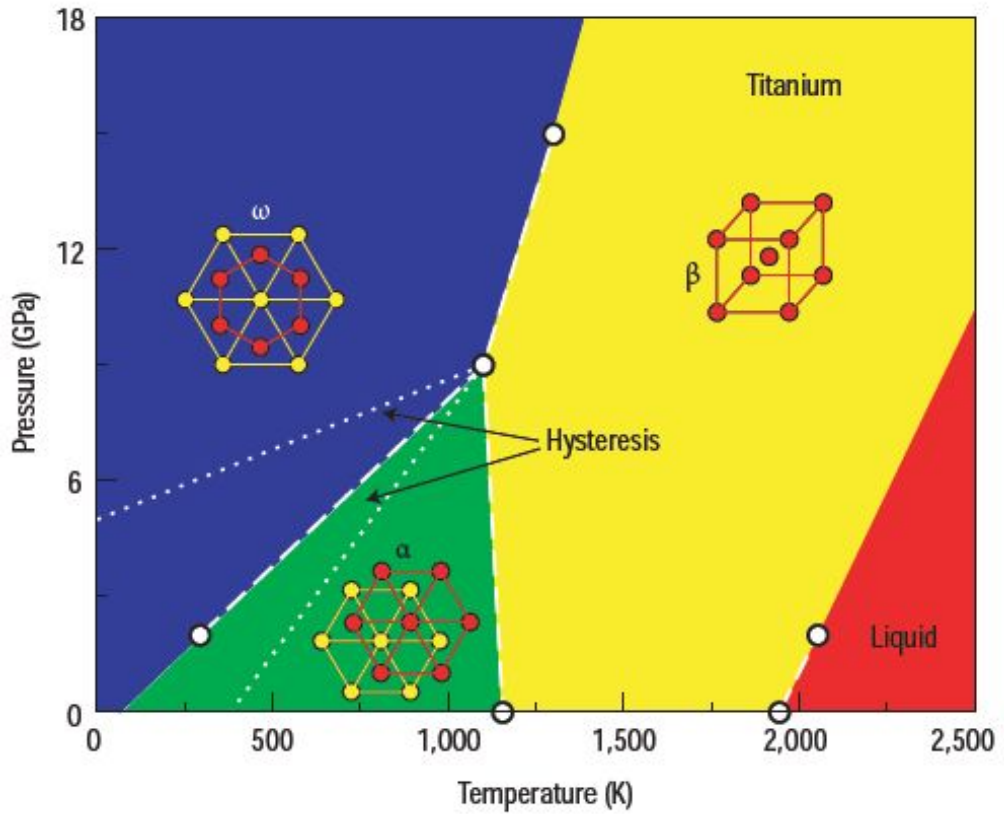


Fig. 1. The phase diagram of titanium as a function of temperature and pressure shows martensitic transformations between the α , β and ω phases[19].

Table 1. Alloying elements of titanium and their effect[23].

	Alloying Element	Effect
1	Aluminum	α stabilizer
2	Tin	α stabilizer
3	Vanadium	β stabilizer
4	Molybdenum	β stabilizer
5	Chromium	β stabilizer
6	Zirconium	α and β strengthener

2.2. Anodization [24]

Currently investigated methods of fabricating titania nanotubes include the assisted-template method, electrochemical anodic oxidation and hydrothermal treatment. A comparison of these three methods along with each their advantages and disadvantages is summarized in Table 2.

Electrochemical anodization is a technique for producing thin oxide films (less than 100 nm) on metals such as titanium, tantalum, aluminum, and zirconium. To accomplish it, dc discharge is set up in an oxygen atmosphere and the substrates are biased positively with respect to the anode. This bias extracts negative oxygen ions from the discharge to the surface, which is also bombarded with electrons that assist the reaction. The process produces very dense, defect-free, amorphous oxide films.

Anodization is a simple and effective method to modify the surface of titanium and its alloys for having biocompatibility and bioactivity. The anodic oxide film exhibits a variety of different properties that rely on the composition and microstructure of the materials and processing parameters, such as anode potential, electrolyte composition, temperature, current and time of anodization.

Table 2. Comparison of titania nanotube fabrication methods[25].

Fabrication method	Advantages	Disadvantages
Template-assisted method	<p>(1) The dimension of nanotubes can be controlled by the dimension and type of templates used</p> <p>(2) Nanotubes formed are of uniform sizes</p> <p>(1) dimension of nanotubes can be controlled by varying voltage, electrolyte, pH and anodizing time</p> <p>(2) Nanotube produced are aligned with a high aspect ratio</p>	<p>(1) Large nanotubes are obtained</p> <p>(2) Time consuming due to prefabrication and post-removal of the templates</p> <p>(3) Contamination may occur during dissolution of template</p> <p>(1) Nanotubes produced are in amorphous phase</p> <p>(2) Annealing is required to crystallize the nanotubes produced but lead to collapse of structure at elevated temperature</p>
Hydrothermal treatment	<p>(1) Pure phase nanotubes with good crystallinity can be obtained</p>	<p>(1) Long reaction time is needed</p> <p>(2) Concentrated NaOH must be employed that can lead to excessive intercalation causing non-aligned nanotubes</p>

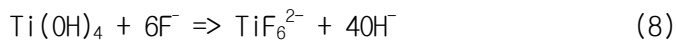
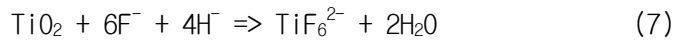
2.2.1. Nanotube formation on the Ti alloy [26]

TiO₂ nanotube arrays are prepared in a two-electrode aqueous electrolyte system by electrochemical anodization (Fig. 2), in which titanium alloy work as anode and metal Pt as a counter cathode. The formation of TiO₂ nanotube thin films starts with oxidizing the metallic surface, which releases Ti⁴⁺ ions and electrons (Eq.(1)). An oxide layer is deposited on the metal surface from the chemical interaction of the released Ti⁴⁺ ions and O²⁻ or OH⁻ ions of water molecules. Eqs. (2) and (3) describe the formation of hydrated anodic and oxide layer. The TiO₂ oxide is produced from the hydrated anodic layer by a condensation reaction (Eq.(4)). At the cathode Pt surface (Eq.(5)), hydrogen evolution generates and the entire process of oxide formation is expressed in Eq.(6).



The fluorine ions in the electrolyte attack the hydrated and oxide layer, where the F⁻ ions are mobile in the anodic layer and react with Ti⁴⁺ under the applied electric field. Field-assisted dissolution of the oxide occurs therefore at the interface between oxide and electrolyte. Localized dissolution of the oxide creates small pits (Eqs.(7) and (8)). These locally etched pits act as pore forming centers, which convert into pores uniformly distributed over the whole surface. The pores start to grow at the pore bottom with inward movement of the oxide layer. Ionic species (F⁻, O²⁻, OH⁻) migrate from the electrolyte toward the metal/oxide interface. The Ti-O bond

undergoes polarization and is weakened to assist dissolution of the metal cations. Ions Ti^{4+} migrating from the metal to the oxide/electrolyte interface dissolve in the HF electrolyte (Eq.(9)). The free O^{2-} anions migrate toward the metal/oxide interface and further interact with the metal (Fig. 2, inset).



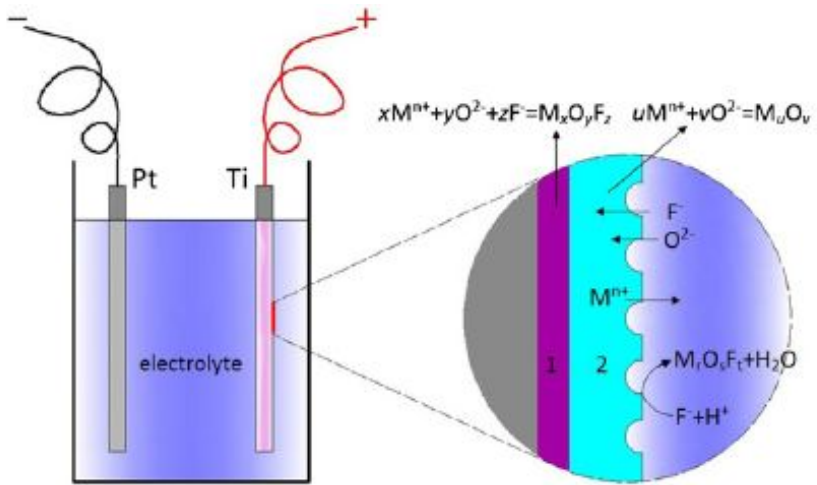


Fig. 2. Anodic growth of the oxide film [26].

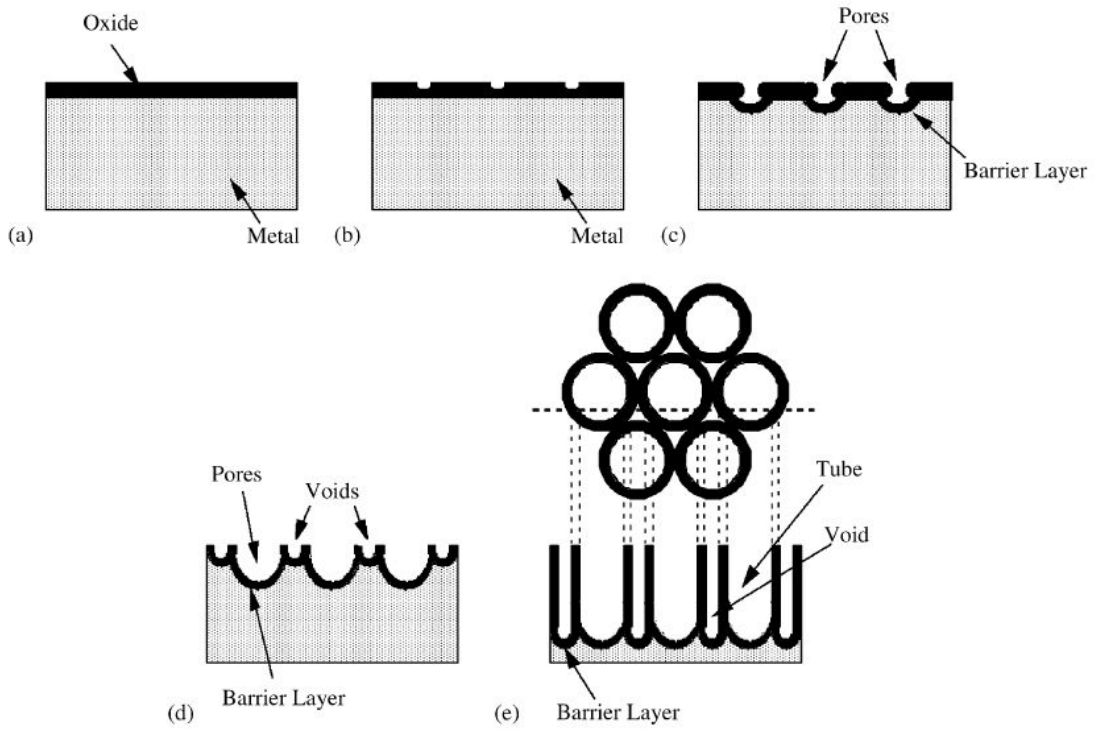


Fig. 3. Schematic diagram of the evolution of a nanotube array at constant anodization voltage: (a) oxide layer formation, (b) pit formation on the oxide layer, (c) growth of the pit into scallop shaped pores, (d) metallic part between the pores undergoes oxidation and field assisted dissolution, and (e) fully developed nanotube array with a corresponding top view[27].

2.3. Hydroxyapatite (HA) [28, 29]

Biologically relevant calcium phosphate (CaP) belong to the orthophosphate group and naturally occur in several biological structures, including teeth and bone. Bone consists of an inorganic component of biological apatites (CaP) and an organic component, consisting primarily of collagen and water. Synthetic hydroxyapatite has been demonstrated to have very similar properties to the naturally occurring mineral component of bones and teeth form of calcium apatites. Consequently, CaP have long been investigated and utilized as coatings for protection against wear corrosion and increased biocompatibility in orthopaedic devices. Table 3 summarizes the calcium phosphate phases, and a brief review of their properties follows below.

Hydroxyapatite theoretically exists as the hydroxyl end-member of apatite, which was suggested in 1912. Hydroxyapatite is one of the apatite structures that were observed in rock, the apatite structure has the basic formula $\text{Ca}_{10}(\text{PO}_4)_6\text{X}_2$. X in the formula is the representation group member of apatite and refers to a hydroxyl (OH) group for hydroxyapatite, a fluoride (F) group for fluorapatite, and a chloride (Cl) group for chlorapatite.

HA is a biomaterial with calcium to phosphorus ratio resembles human bone. So, it has been used as a bone replacement material in restorative dental and orthopedic implants. HA can improve bonding strength between body tissues and an implant surface. Also. HA as an implant can bond and promote natural tissue growth.

Table 3. The calcium phosphate phases used to date for coatings in orthopaedic devices[28].

Name	Formula	Ca/P ratio
Calcium phosphate dihydrate(brushite)	$\text{CaHPO}_4 \cdot 2\text{H}_2\text{O}$	1.0
Anhydrous calcium phosphate(monetite)	CaHPO_4	1.0
Octacalcium phosphate	$\text{Ca}_8\text{H}_2(\text{PO}_4)_6 \cdot 5\text{H}_2\text{O}$	1.33
Tricalcium phosphate(whitlockite)	$\text{Ca}_3(\text{PO}_4)_2$	1.5
Fluorapatite	$\text{Ca}_{10}(\text{PO}_4)_6\text{F}_2$	1.67
Hydroxyapatite	$\text{Ca}_{10}(\text{PO}_4)_6(\text{OH})_2$	1.67

2.4. Surface treatment method for HA coating [30]

Surface treatment methods are classified according to their processes and purposes. Major purpose of surface modification is to improve hard tissue compatibility or accelerate bone formation. Research to improve hard tissue compatibility involves two approaches based on the resultant surface layer: a calcium phosphate and Ti oxide layer with the thickness measured in micrometers and a surface-modified layer with the thickness measured in nanometers. Fig. 4 shows the history of the surface treatment technique to improve hard tissue compatibility. Surface property is particularly significant for biomaterials, and thus surface modification techniques are particularly useful to biomaterials. Dry process (using ion beam) and wet process (which is performed in aqueous solutions) are predominant surface modification techniques. In particular, electrochemical technique in the wet process is important near recently. HA coating on metallic materials is widely used to form the HA layer—which is the nucleus for active bone formation and conductivity. Electrochemical deposition of HA coating on Ti surface has unique advantages, which is an attractive process because highly complex objects can be coated relatively quickly at low process temperatures. However, the HA-Ti interface or HA itself may fracture under relatively low stress because of low interface bonding strength and low toughness. The crystallinity of a thin film formed with ion beam is low and the solubility is large. The crystallinity of coated HA is an important factor because crystallinity governs solubility in the human body. Low crystalline film on Ti dissolves rapidly when the Ti is implanted into a human body. Thus heat treatment of HA film is necessary to increase its crystallinity and reduce its solubility. Calcium ions are implanted during the mixing process to induce strong bonding between the HA film and the Ti substrate, with implanted calcium ions serving as binders. HA and calcium phosphate can coating by RF magnetron sputtering.

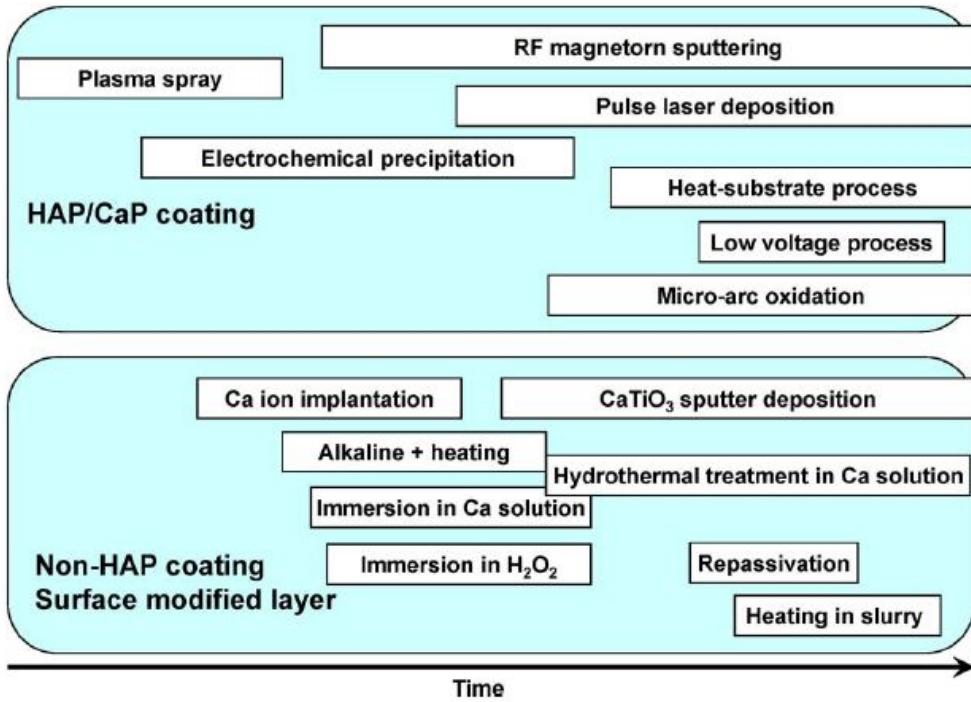


Figure. 4. History of surface treatment technique to improve hard tissue compatibility. Approaches to improving hard tissue compatibility are categorized based on the resultant surface layer: calcium phosphate layer formation with thickness measured in micrometers and surface-modified layer formation with thickness measured in nanometers[30].

Table 4. Different technique to deposit HA coatings.[31]

Technique	Thickness	Advantages	Disadvantages
Thermal spraying	30–200 μm	High deposition rates; low cost	Line of sight technique; high temperatures induce decomposition; rapid cooling produces amorphous coatings
Sputter coating	0.5–3 μm	Uniform coating thickness on flat substrates; dense coating	Line of sight technique; expensive time consuming; produces amorphous coatings
Pulsed laser deposition	0.05–5 μm	Coating with crystalline and amorphous; coating with dense and porous	Line of sight technique
Dynamic mixing method	0.05–1.3 μm	High adhesive strength	Line of sight technique; expensive; produces amorphous coatings
Dip coating	0.05–0.5 mm	Inexpensive; coatings applied quickly; can coat complex substrates	Requires high sintering temperatures; thermal expansion mismatch
Sol-gel	< 1 μm	Can coat complex shapes; Low processing temperatures; relatively cheap as coatings are very thin	Some processes require controlled atmosphere processing; expensive raw materials
Electrophoretic deposition	0.1–2.0 mm	Uniform coating thickness; rapid deposition rates; can coat complex substrates	Difficult to produce crack-free coatings; requires high sintering temperatures
Biomimetic coating	< 30 μm	Low processing temperatures; can form bonelike apatite; can coat complex shapes; can incorporate bone growth stimulating factors	Time consuming; Requires replenishment and a constant of pH of simulated body fluid
Hot isostatic pressing	0.2–2.0 mm	Produces dense coatings	Cannot coat complex substrates; high temperature required; thermal expansion mismatch; elastic property differences; expensive; removal/interaction of encapsulation material

2.4.1 Electrochemical deposition of HA

Electrochemical deposition is used to form an HA layer on Ti. Through an electrochemical process, carbonate-containing HA with a desirable morphology such as plate, needle, and particle could be precipitated on a Ti substrate, which is heated to get a better coating layer. β -TCP is cathodically coated on Ti for immobilization of collagen. Low-voltage alternating current affect also to precipitate calcium phosphate on Ti. This technique is useful for the treatment of substrate without the dissolution of Ti. HA is electrodeposited with pulse current. Nano-grained calcium phosphate is electrochemically deposited on Ti using acidic electrolytes. The coating layer contains dicalcium phosphate dihydrate (55–85 nm in grain size) with a small amount of HA (20–25 nm); the content of HA increases with the increase of the current density. An electrochemical method of producing nanocrystalline HA coatings on Ti surface is reported. Also, HA is coated by dynamic voltage during electrochemical deposition.

2.4.2 The sputtering process for HA coating [32]

Sputtering technique is commonly used for thin-film deposition, etching and analytical techniques. There are different ways to perform sputtering, DC-diode, RF-diode (radio frequency) and magnetron sputtering being the three main processes. In DC-diode sputtering, the difference in potential generated by a DC power supply will create an electrical field between the two electrodes, and in the presence of an inert gas, the ionization process occurs via electron collisions that form a plasma in the intermediate regions. However, in a DC-sputtering system, via the simple substitution of a metal target with an insulator target, the sputtering glow discharge cannot be sustained, because of the immediate build-up of a surface charge of positive ions on the front side of the insulator. To sustain the glow discharge with an insulator target, the DC power supply should be replaced with an RF power supply, and an impedance matching network should be implemented. This system is called RF-sputtering. Fig. 5(a - c) shows a representative sputtering system, in which the target and magnetrons, along with details, substrate positions, vacuum pumps, power supplies, plasma and the physical ejection of atoms from the target to the substrate surface, can be seen. Due to the applied electric field, the electrons follow helical paths around the magnetic field lines, undergoing more ionizing collisions with gaseous neutrals near the target surface than would otherwise occur.

Sputter deposition of hydroxyapatite on titanium substrates was performed in two steps: (1) plasma etching of hydroxyapatite target, (2) sputter deposition of hydroxyapatite on titanium substrates. HA deposit on Ti surface by magnetron sputtering suggest that the strong bonding between the HA and Ti layers.

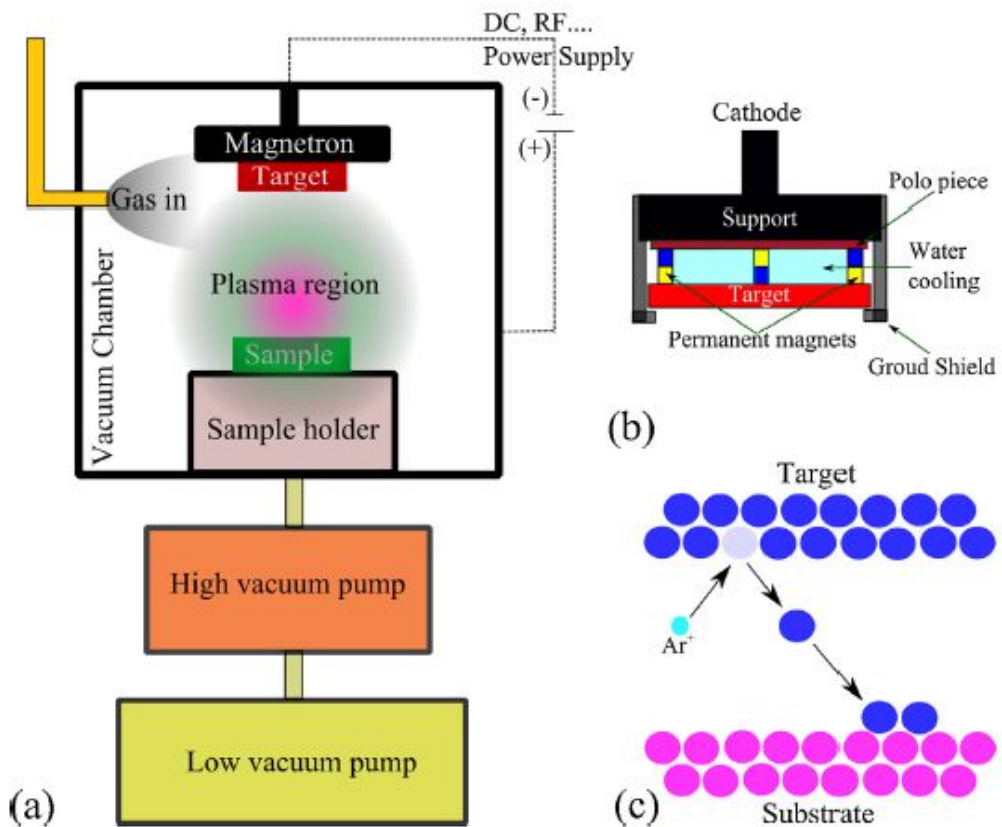


Fig. 5. Schematic diagram of the sputter system: (a) Representative scheme of a typical magnetron sputtering system. (b) Details of the magnetron. (c) Representative scheme of the physical ejection of atoms from the target to the substrate surface[31].

III . MATERIALS AND METHODS

3.1. Preparation of Ti-25Ta-xZr alloys

Ti-25Ta-xZr alloys were prepared from Ti (Grade 4, G&S Ti, USA), Ta (99.95% purity, Kurt J. Lesker Company, USA), and Zr (99.95% purity, Kurt J. Lesker Company), with Zr contents from 0, 3, 7 and 15 wt. %. Each alloy was melted twenty times in an arc-melting vacuum furnace under high purity argon atmosphere, because of the large differences in the melting temperatures of the three constituents and their reactive nature with air. Heat treatment was performed at 1000°C for 12 h in an argon atmosphere in order to homogenize, followed by quenching into 0°C water. All alloys were then cut into samples having 10 mm diameter and 2.5 mm thickness. Specimens for metallographic examination were polished with SiC papers ranging from 100 to 2000 grit, finishing with a suspension of 0.3 μm Al_2O_3 slurry. All polished samples were ultrasonically cleaned to remove grease and other surface contaminants.

3.2. Analysis of surface characteristics for Ti-25Ta-xZr alloys

The phase and composition of the Ti-25Ta-xZr alloys surfaces were determined by using an X-ray diffractometer (XRD, X`pert PRO, Philips). Ni-filtered Cu $K\alpha$ radiation was used in this study. Phase was identified by matching each characteristic peak with JCPDS files. The Ti-25Ta-xZr alloy surfaces, nanotube surfaces and HA coated nanotubular surfaces were observed by optical microscopy (OM, oympus, BX 60M, Japan), field-emission scanning electron microscopy (FE-SEM, Hitachi, 4800, Japan) and energy dispersive x-ray analysis (EDS, Oxford ISIS 310, England). The etching treatment was

performed in Keller's reagent (2 ml HF + 3 ml HCl + 5 ml HNO₃ + 190 ml H₂O).

3.3. Nanotubular oxide formation on the alloy surface

The electrochemical experiments were carried out with a conventional three electrode configuration that platinum counter electrode, saturated calomel reference electrode and anode working electrode. Before anodization, the sample was embedded with epoxy resin, leaving a square surface area of 10mm^2 exposed to the anodizing electrolyte. All nanotube formation experiments were carried out at constant voltage (30 V) for 1h (potentiostat 362, EG&G Company, USA). The electrolyte was composed of 1 M H_3PO_4 containing 0.8 wt.% NaF.

The morphology of the porous Ti oxide was characterized by a field-emission scanning electron microscopy (FE-SEM, Hitachi S-4800, Japan).

3.4. HA coating on nanotubular Ti-25Ta-xZr alloys by electrochemical deposition method

Electrochemical deposition of HA on nanotubular Ti-25Ta-xZr surface was carried out using cyclic voltammetry (CV) method at 80°C in 5 mM Ca (NO₃)₂ + 3 mM NH₄H₂PO₄. CV was carried out using the three electrode configuration by scanning the potential between 0 V and -1.5 V at scan rate 0.5 V/s. The electrochemical setup consisted of a three-electrode configuration with the alloy, a platinum electrode as counter electrode, an SCE (saturated calomel electrode) as reference electrode, and samples as working electrode, respectively. The pulsing cycle and condition of electrochemical deposition was schematically illustrated in Fig. 6 and Table 5.

Table 5. Electrochemical HA precipitation condition.

Type of applying potential	Cyclic voltammetry(CV)
Electrolyte	Ca(NO ₃) ₂ , NH ₄ H ₂ PO ₄
Working electrode	Sample
Counter electrode	Carbon
Reference electrode	SCE
Temperature	80°C ± 1
Scan rate	0.5 V/s
Cycles	50

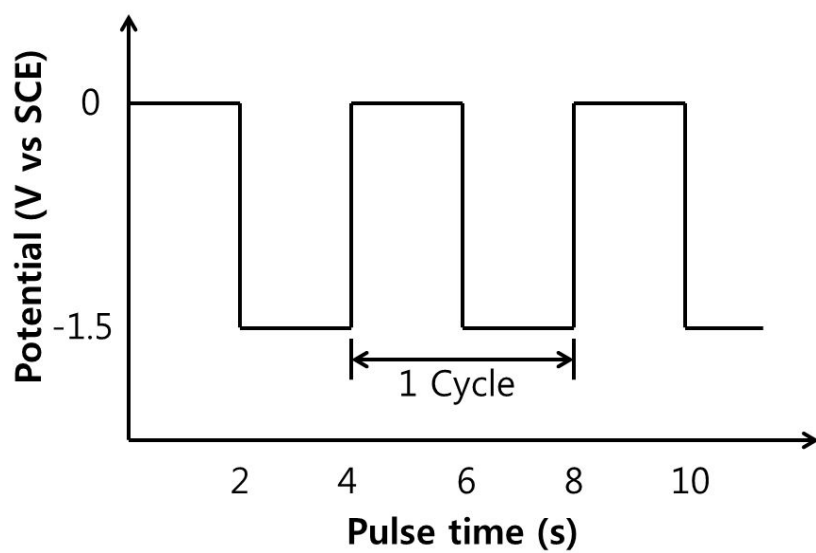


Fig. 6. Process of monitoring voltage versus times during electrochemical HA deposition.

3.5. HA coating by the radio-frequency(RF) magnetron sputtering

PVD coating were obtained by the ratio-frequency (RF) magnetron sputtering system. The RF power was 45 W, the working pressure was kept at 10×10^{-3} Torr. During sputtering for HA, a reactive gas of argon (Ar: 40 sccm) was used for deposition onto the metal alloy plate. Pre-sputtering and deposition times were 20 and 120 min, respectively.

Surface morphologies of the HA coating on the nanotubular Ti-25Ta-xZr alloys were observed using by field emission scanning electron microscopy (FE-SEM, Hitachi 4800, Japan). In order to identify the composition of HA coated Ti-25Ta-xZr alloys were characterized by energy dispersive X-ray spectroscopy (EDS).

Table 6. The coating condition of RF sputtering.

Coating condition	
Equipment	RF Sputtering
Target	HA
Base Pressure	10^{-6} Torr
Working Pressure	10^{-3} Torr
Gas	Ar (40 sccm)
Pre-sputtering	20 min
Deposition Time	2 hr
Power Supply	45 W

3.6. Surface wettability test

Surface wettability test was carried out on the bulk surface, nanotubular surface, and HA coated nanotubular surface using a contact angle goniometer (Surfacetech GSA, Korea) in sessile drop mode 5 μ L water drops.

IV. RESULTS AND DISCUSSION

4.1. Microstructures of Ti-25Ta-xZr alloys

Fig. 7 and Fig. 8 show the microstructures of the Ti-25Ta-xZr alloys surface with different Zr content (0, 3, 7 and 15 wt.%) after heat treatment at 1000 °C for 12h in Ar atmosphere, followed by 0 °C water quenching. The microstructures of Ti-25Ta(a), Ti-25Ta-3Zr(b) and Ti-25Ta-7Zr(c) show mainly martensite structure. But, the microstructure of Ti-25Ta-15Zr(d) shows mainly an equiaxed structure. On the other hand, the martensite appearance was decreased, by increasing the Zr content. Microstructures of Ti-25Ta-xZr alloys were changed from α'' phases to β phases with Zr content. The quenched Ti-Ta alloy has the hexagonal (α') martensitic structure for Ta contents up to 26 wt. %; the orthorhombic (α'') martensite forms with Ta contents in the range of 26-52 wt. %; and the single-phase metastable bcc (body-centered cubic) β structure exists when the Ta content is greater than 65 wt. % [33]. Also, the effect of Zr content in these β -type Ti alloys might be increased in the compositional ratio of β -stabilizing elements in β -type Ti alloy caused by the addition of the neutral element Zr [34]. Because the microstructure of the Ti-25Ta-xZr is strongly changed by Zr contents, the present study suggests that phase transformation in the Ti-25Ta-xZr alloys is sensitive to Zr content.

Fig. 9 shows the peaks on the XRD patterns of the homogenized Ti-25Ta-xZr alloys. The XRD peaks were identified using the JCPDS diffraction data for element standards. In Fig. 9, β peak (2 Theta = 38°) increased as Zr content increased, whereas, α peak (2 Theta = 62°) decreased. Also, α peak (2 Theta = 70°) translated β peak (2 Theta = 69°) as Zr content increased. Therefore, transformation from α'' to β was gradually progressed with increasing Zr content due to Zr displacement [35]. It is confirmed that

Zr element in Ti-Ta-Zr system plays role as a β -stabilizing element. Although Zr is not considered to a strong β -stabilizing element in Ti alloys, its addition caused displacement of the martensitic transformation temperature that is usually attributed to β -stabilizing elements [35]. It is reported that the amount of α'' phase increases with increasing cooling rate due to the transformation of β phase into α'' phase. As a result, the microstructures and XRD patterns of Ti-25Ta-xZr alloys were strongly dependent on the amount of Zr and the β -stabilizing effect of Zr increased with increasing relative proportion of the other β -stabilizing element such as Ta in the alloy. Therefore, as mentioned before, phase transformation in the Ti-25Ta-xZr alloys was sensitive to Zr content.

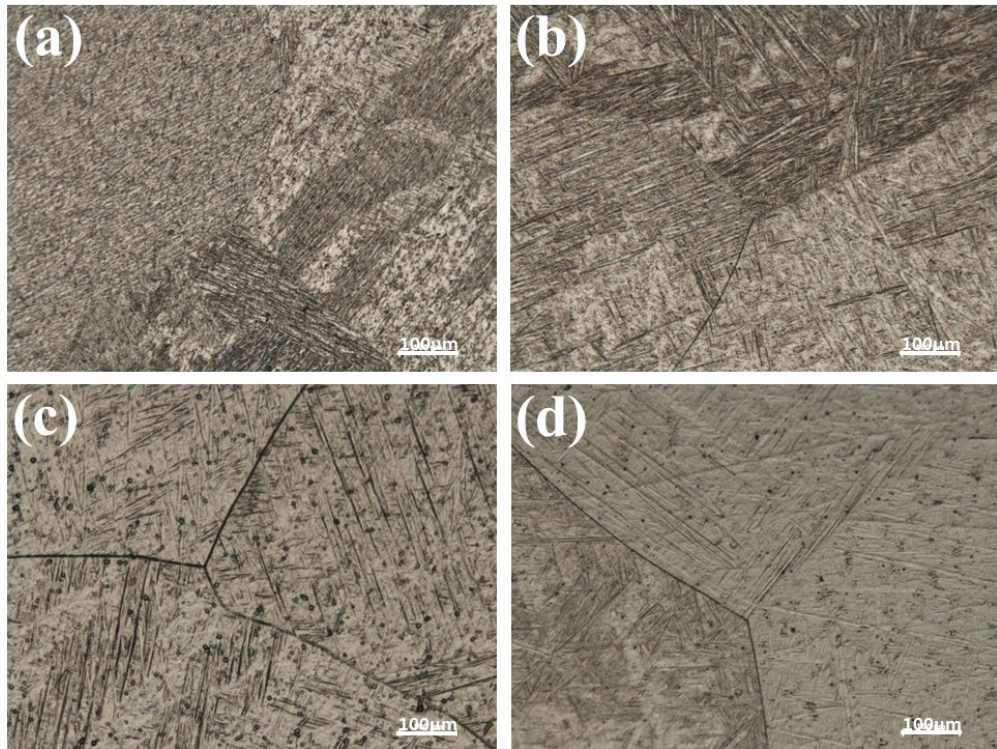


Fig. 7. OM images of Ti-25Ta-xZr alloys after heat treatment at 1000 °C for 12 h in Ar atmosphere, followed by 0 °C water quenching: (a) Ti-25Ta, (b) Ti-25Ta-3Zr, (c) Ti-25Ta-7Zr, (d) Ti-25Ta-15Zr.

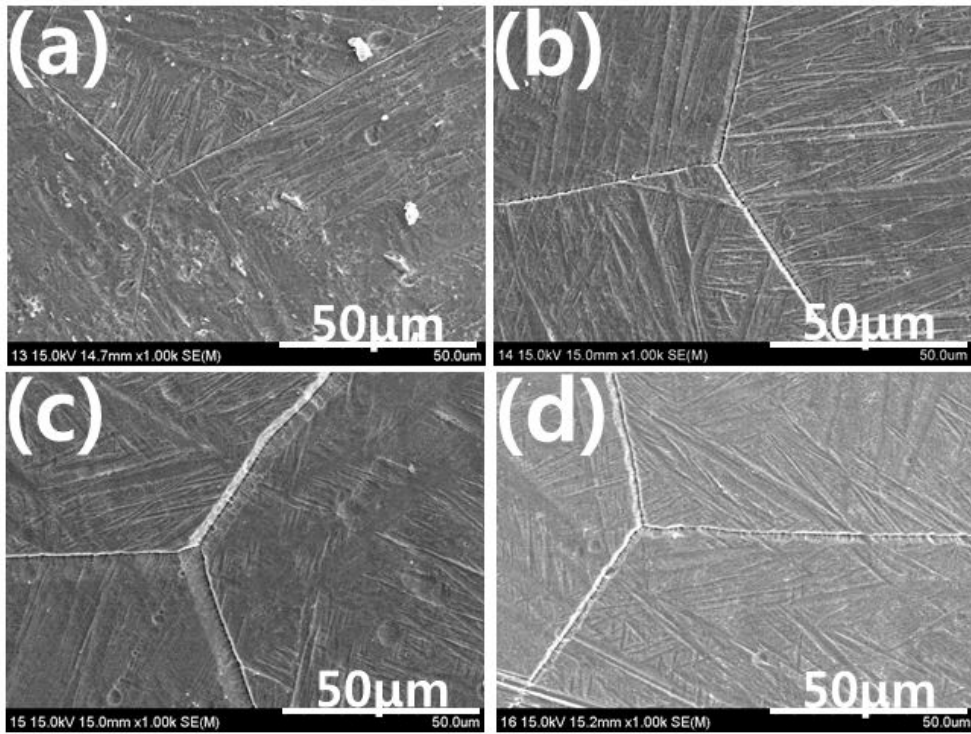


Fig. 8. FE-SEM images of Ti-25Ta-xZr alloys after heat treatment at 1000 °C for 12 h in Ar atmosphere, followed by 0 °C water quenching: (a) Ti-25Ta, (b) Ti-25Ta-3Zr, (c) Ti-25Ta-7Zr, (d) Ti-25Ta-15Zr.

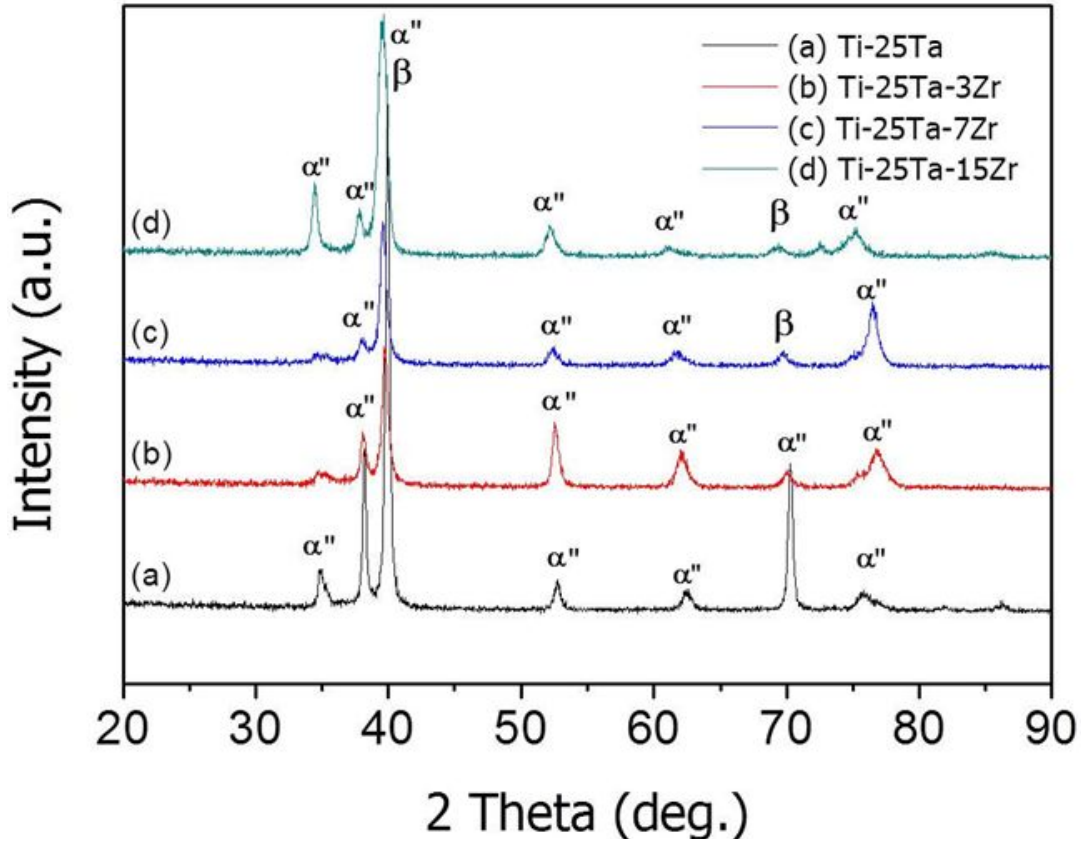


Fig. 9. XRD peaks of Ti-25Ta-xZr alloys after heat treatment at 1000 °C for 12 h in Ar atmosphere, followed by 0 °C water quenching: (a) Ti-25Ta, (b) Ti-25Ta-3Zr, (c) Ti-25Ta-7Zr, (d) Ti-25Ta-15Zr.

4.2. The nanotubular structure of Ti-25Ta-xZr alloy

Fig. 10 shows FE-SEM images of top views Fig. 10(a - d), bottom views Fig. 10(e - h), and cross-section views Fig. 10(i - l) of nanotubes formed on the Ti-25Ta-xZr alloys, respectively. The diameters of the small nanotubes increased with Zr content, whereas the diameters of the large nanotubes decreased with Zr content. The nanotube diameters on Ti-25Ta, Ti-25Ta-3Zr, and Ti-25Ta-7Zr show a somewhat irregular distribution, whereas the nanotubes on Ti-25Ta-15Zr have a more regular pattern of large tubes surrounded by smaller tubes. These phenomena suggest that Zr has a role in the formation of a stable film that protect attack from fluorine ion, and that areas devoid of nanotubes acted as subsequent nucleation sites for the smaller tubes [36]. Also the arrangement of several smaller tubes around the large tube became more highly ordered as the Zr content increased. The stable oxide film as ZrO_2 and Ta_2O_5 films on the Ti-Ta-Zr alloy surface can interrupt formation of nanotubes and retard their growth in fluorine solution [35]. So, the shapes and dimensions of the nanotubular structure, which contains TiO_2 , Ta_2O_5 and ZrO_2 can be controlled by the range in dissolution parameters. Also, Ta_2O_5 , and ZrO_2 have much lower chemical dissolution rate than TiO_2 in electrolytes containing F^- ions, the dissolution of the nanotubes is interrupted once they are formed permitting the formation of a longer nanotubular structure [37, 38]. The results indicated that the composition of the Ti-25Ta-xZr alloys had a major influence on formation of this two-size scale, which appeared predominantly with an increase in Zr content [1, 4]. Thus, our results confirm that the composition of the Ti-25Ta-xZr alloys has a major influence on the formation of a two-size population of nanotubes .Fig.10 (i), (j), (k) and (l) presenting the cross-sectional FE-SEM images of the samples show that as the Zr content increased from 0 to 15 wt. %, the average length of the nanotubes generally increased (3.4 μ m, 3.5 μ m, 4.3 μ m and 6.3 μ m, respectively). This

phenomenon that the formation of higher aspect-ratio nanotubes is more ordered by increasing the Zr content is attributed to equilibrium processes involving chemical dissolution rates during anodization. It is evident that the amount of Zr in the ternary Ti-25Ta-xZr alloys strongly controls the nanotube length.

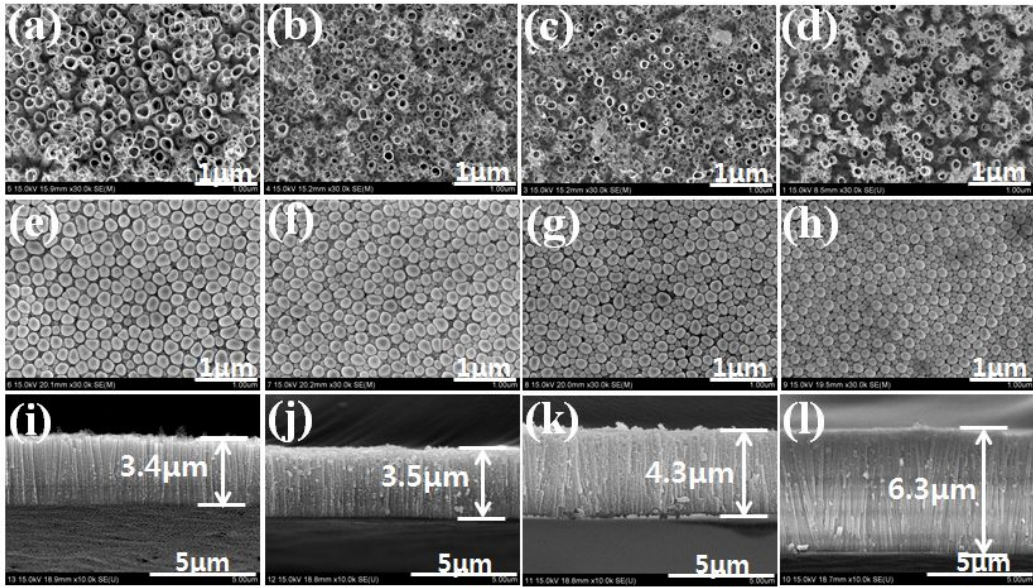


Fig. 10. FE-SEM images of top, bottom, and cross-section for TiO_2 nanotubes formed on Ti-25Ta-xZr alloys: (a), (e) and (i) Ti-25Ta; (b), (f) and (j) Ti-25Ta-3Zr; (c), (g) and (k) Ti-25Ta-7Zr; (d), (h) and (l) Ti-25Ta-15Zr.

4.3. The HA coating on nanotubular Ti-25Ta-xZr alloys by electrochemical deposition method

Fig. 11 shows FE-SEM images of hydroxyapatite coating on nanotube formed Ti-25Ta-xZr alloys in 5 mM $\text{Ca}(\text{NO}_3)_2$ + 3 mM $\text{NH}_4\text{H}_2\text{PO}_4$ electrolyte with 50 cycle of potential. Fig. 11 (a - d) shows HA coated film on nanotubular Ti-25Ta, Ti-25Ta-3Zr, Ti-25Ta-7Zr, and Ti-25Ta-15Zr alloys, respectively. Fig. 11 (e - h) and (i - l) show high magnification of Fig. 11 (a - d) with 30k and 100k. Fig. 11 (a) and (b) were observed leaf like precipitation above nanotube. Fig. 11 (c) and (d) were observed a lot of needle like precipitation. The tip of nanotube were covered with HA precipitates, HA film was well spread on the surface. Also, with increasing Zr content, leaf like shapes transferred to the needle like precipitates. Morphology of HA coating on nanotube may be affected by microstructure and nanotube morphology. So we researched analysis of pore and wall surface ratio, with increasing Zr content.

Fig. 12 shows top view FE-SEM images and EDS peak for HA coated film on nanotubular Ti-25Ta-xZr alloys, respectively. From the EDS results of Fig. 12 (a), Ti, Ta, Ca and P were detected in the coated layer, from the EDS results of Fig. 12 (b), (c) and (d), Ti, Ta, Zr, Ca and P were detected in the coated layer. This composite layer is possible role as a hybrid coating materials, that is, Ti plays a role to increase the bonding strength between substrate, and HA composite layer can contribute the surface for bioactivity on the implant surface [39].

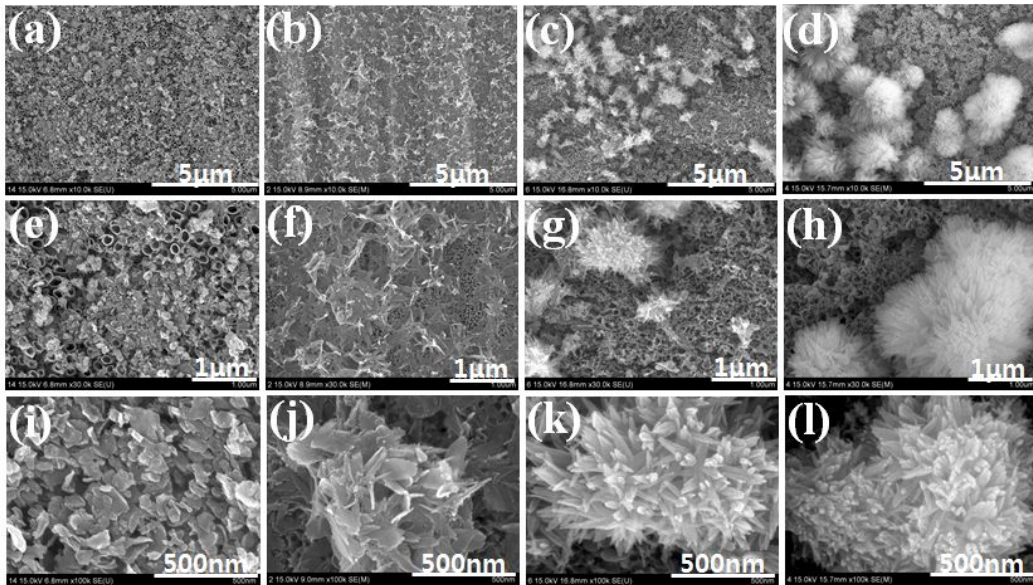


Fig. 11. FE-SEM top view images of the HA coated film on nanotubular Ti-25Ta-xZr alloys by electrochemical deposition: (a), (e) and (i) Ti-25Ta; (b), (f) and (j) Ti-25Ta-3Zr; (c), (g) and (k) Ti-25Ta-7Zr; (d), (h) and (l) Ti-25Ta-15Zr.

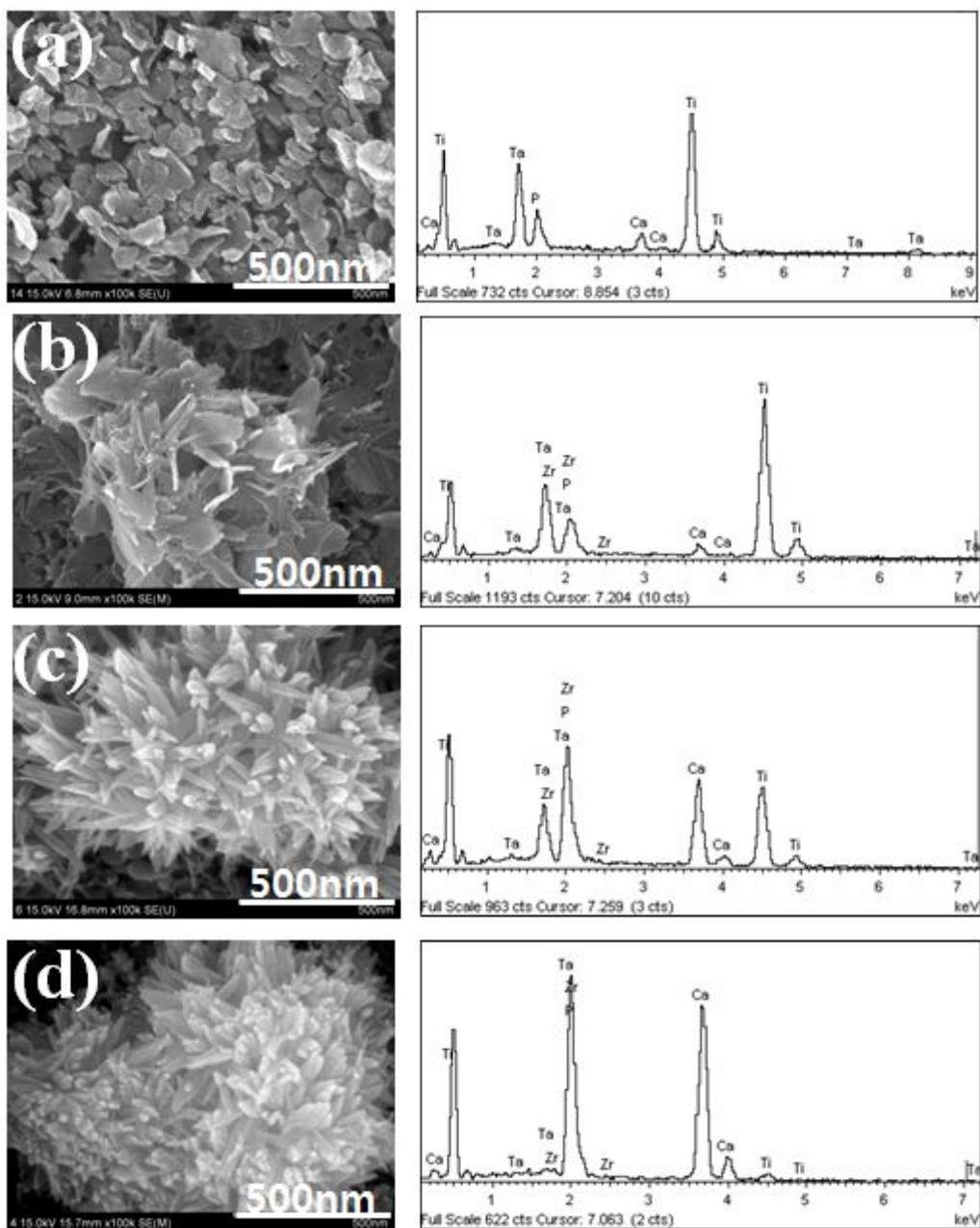


Fig. 12. FE-SEM images and EDX analyses of the HA coated film on nanotubular Ti-25Ta-xZr alloys by electrochemical deposition: (a) Ti-25Ta, (b) Ti-25Ta-3Zr, (c) Ti-25Ta-7Zr, (d) Ti-25Ta-15Zr.

Fig. 13 (a) and (b) show FE-SEM images of bottom view for nanotubes formed on Ti-25Ta, Ti-25Ta-15Zr, respectively. Fig. 13 (c) and (d) show analysis of pore and wall surface for nanotubes formed on Ti-25Ta, Ti-25Ta-15Zr, respectively. The result of analysis shows in Table 7. As Zr content increased, black pixel (pore wall) decreased. Whereas, white pixel (pore) increased.

Fig. 14 shows schematic diagram of the HA coated film on nanotubular Ti-25Ta-xZr alloys. As mentioned above Fig. 13, occupied percent of pore wall surface for Ti-25Ta alloy decreased compared to Ti-25Ta-15Zr alloy. Namely, Ti-25Ta alloy have a lot of region of pore wall surface compared to Ti-25Ta-15Zr alloy. So HA precipitation may be preferentially covered in pore wall surface. And then, the HA precipitate was stacked on top of covered HA precipitation, repeatedly. Finally, leaf like shape was form on the nanotubular Ti-25Ta alloy. Whereas, regular pattern having nanotube as Ti-25Ta-15Zr Alloy have little pore wall surface. Therefore, HA precipitation may grow from the edge of nanotubes. Finally, rose like shape was formed on the nanotubular Ti-25Ta-15Zr alloy.

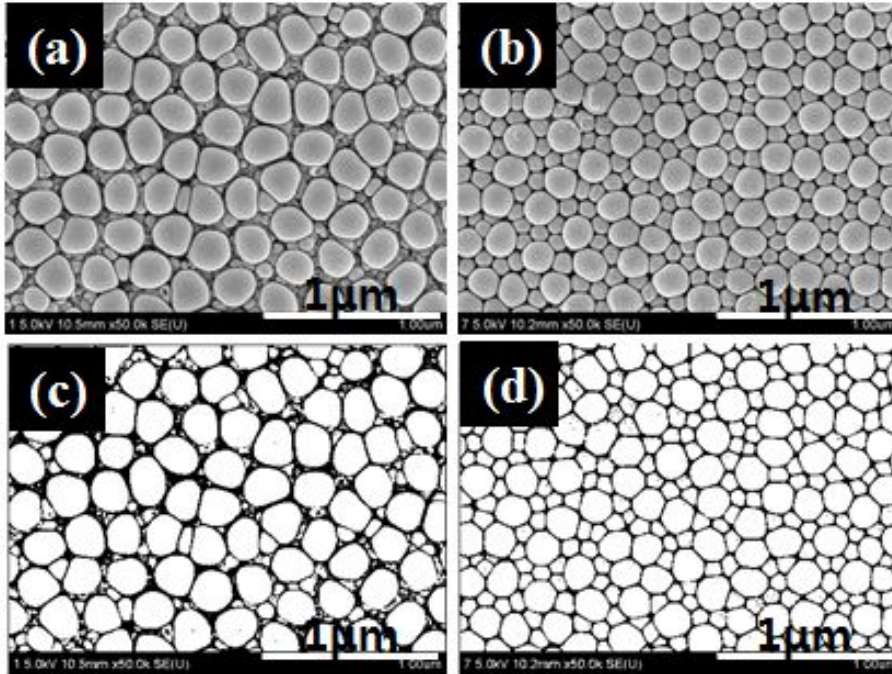


Fig. 13. FE-SEM images of pores and pore wall surface areas on nanotube layers (a), (c); Ti-25Ta, (b), (d); Ti-25Ta-15Zr.

Table 7. Volume ratio of pores and pore wall surface areas on nanotube layers.

	Black Pixel	White Pixel	Black/White(%)
0Zr	33239	82991	28.598/71.402
15Zr	27018	89212	23.245/76.755

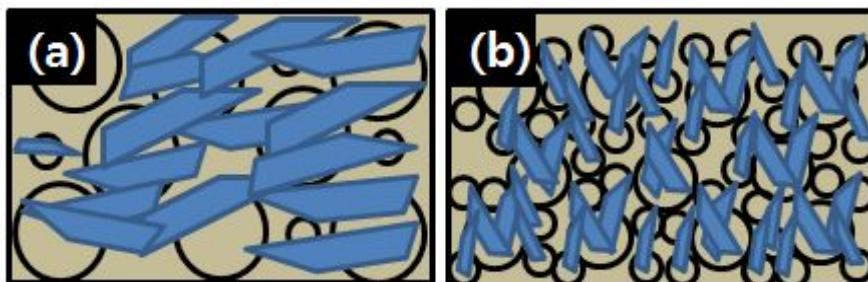


Fig. 14. Schematic diagram of the HA coated film on nanotubular Ti-25Ta-xZr alloys: (a) Ti-25Ta, (b) Ti-25Ta-15Zr.

4.4. The RF-sputtered HA coating on HA deposited Ti-25Ta-xZr alloys

Fig. 15 shows FE-SEM images of RF-sputtered HA coating after HA deposition on nanotubular Ti-25Ta-xZr alloys. Fig. 15 (a - d) shows the top view of RF-sputtered HA coating on nanotubular Ti-25Ta, Ti-25Ta-3Zr, Ti-25Ta-7Zr and Ti-25Ta-15Zr alloys, respectively. Fig. 15 (e - h) and (i - l) show high magnification of Fig. 15 (a - d) with 30k and 100k. Surface of RF-sputtered HA coating on HA deposited on nanotubular Ti-25Ta-xZr alloys were covered entirely with the HA film. In the case of HA coated nanotubular Ti-25Ta-xZr alloys by electrochemical method, nanotubes were partially non-covered and covered with HA film. But, after sputtered HA coating on Ti-25Ta-xZr alloys, all nanotubes were covered with HA film as shown in Fig.15. It is thought that uncovered pore can be covered with HA by sputtering and entirely covered HA film surface has good for biocompatibility compared to entirely uncovered HA film surface.

Fig. 16 shows FE-SEM top view images and EDS peak for RF-sputtered HA coating film after HA deposition on nanotubular Ti-25Ta-xZr alloys, respectively. From the EDS results of Fig. 16 (a), Ti, Ta, Ca and P were detected in the coated layer, and from the EDS results of Fig. 16 (b), (c) and (d), Ti, Ta, Zr, Ca and P were detected in the coated layer.

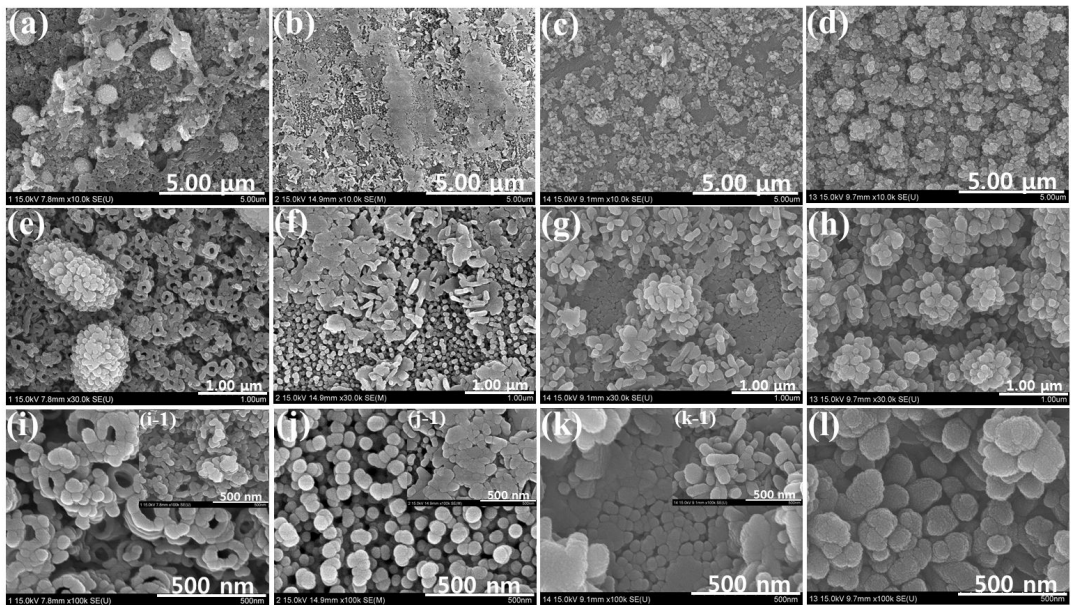


Fig. 15. FE-SEM top view images of the RF-sputtered HA coating on HA deposited Ti-25Ta-xZr alloys: (a), (e) and (i) Ti-25Ta; (b), (f) and (j) Ti-25Ta-3Zr; (c), (g) and (k) Ti-25Ta-7Zr; (d), (h) and (l) Ti-25Ta-15Zr.

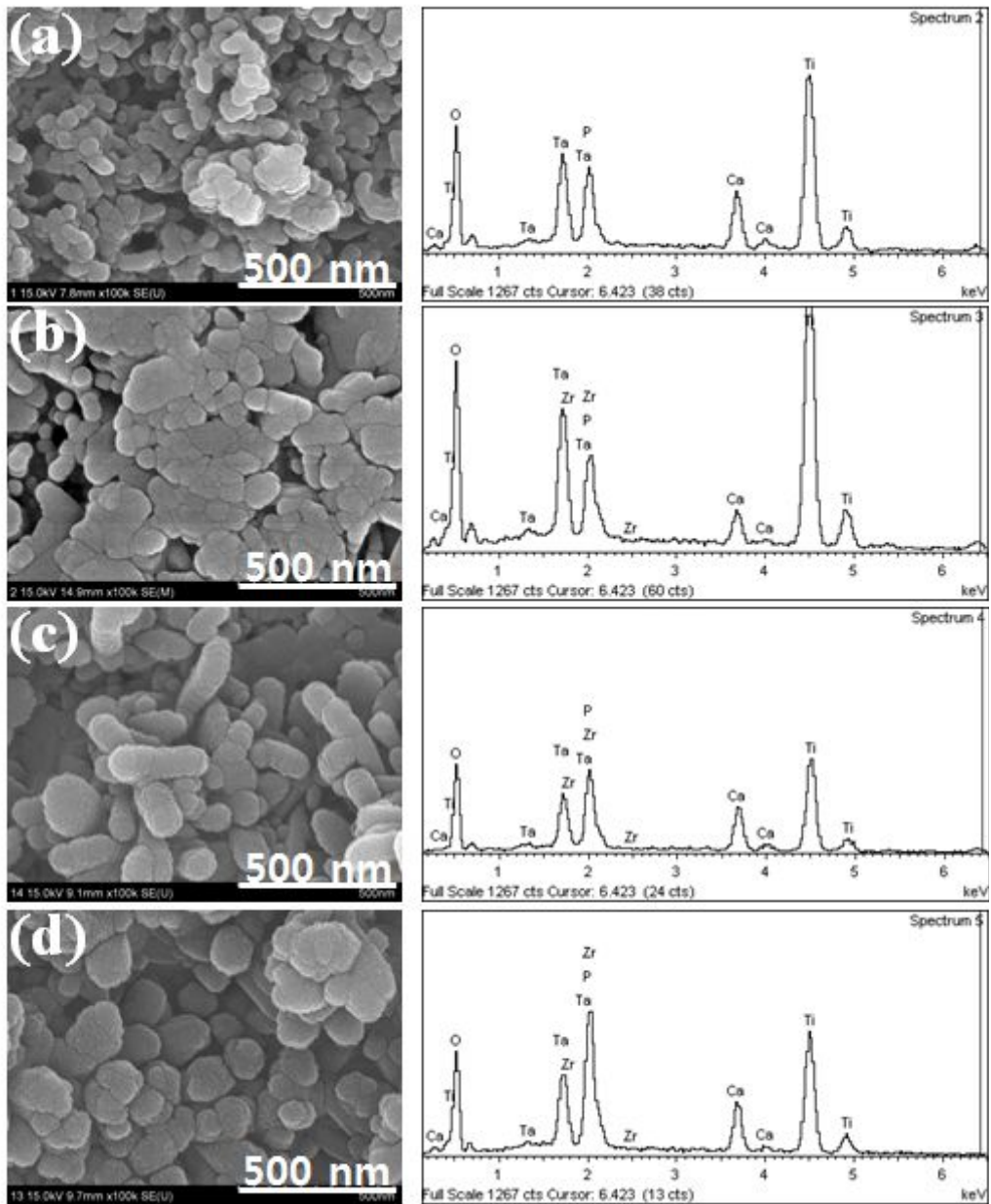


Fig. 16. FE-SEM images and EDX analyses of the RF-sputtered HA coating on HA deposited Ti-25Ta-xZr alloys: (a) Ti-25Ta, (b) Ti-25Ta-3Zr, (c) Ti-25Ta-7Zr, (d) Ti-25sTa-15Zr.

4.5. Wettability of Ti-25Ta-xZr alloys with various surface modification

Fig. 17 (a), (b) and (c) show the contact angle values for Ti-25Ta-15Zr alloys with different surface treatment; bulk surface, the nanotube-formed surface, and HA coated on nanotubular surface, respectively. The surface treatment changes the surface wettability. The value of contact angle indicates that the surface is hydrophilic or hydrophobic. Therefore, wettability test is one of the most important parameters for biomaterials. The contact angle of HA coated on nanotubular Ti-25Ta-15Zr alloys exhibited the lowest contact angle with 3.94° . The HA coated nanotubular surface show the improved wettability compared to bulk and nanotube surface. Because HA coated nanotubular surface increase the surface energy of interface between HA coated surface and vapor due to lead to hydrophilic nature of the nanoporous surface [40]. This means very high wettability (hydrophilic property) and biocompatibility, whereas the bulk alloy surface without the nanotubes has a very high contact angle value of 61.59° . Accordingly, HA coated on nanotubular surface can give the bioactivity for the implant surface and provide the pathways for cell through the tube like a lamellopodia. HA coated on nanotubular morphology is important for cell proliferation and adhesion on the implant surface [40].

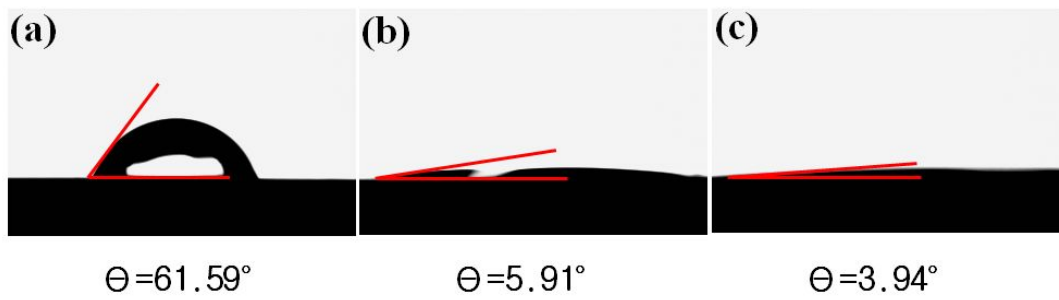


Fig. 17. Contact angle and snap shot of wettability on the surfaces: (a) Ti-25Ta-15Zr alloy, (b) nanotube formed Ti-25Ta-15Zr alloy, (c) HA coated nanotubular Ti-25Ta-15Zr alloy.

V. CONCLUSIONS

In this study, hydroxyapatite coating on nanotubular Ti-25Ta-xZr alloys by RF-sputtering after electrochemical deposition for biomaterials have been researched.

The results were as follows;

1. Microstructures of Ti-25Ta, Ti-25Ta-3Zr, and Ti-25Ta-7Zr alloys were shown martensite structure. But Ti-25Ta-15Zr alloy were shown equiaxed structure. and α phase decreased, whereas β phase increased as Zr content increased.
2. As Zr content increased, the arrangement of nanotube changed irregular distribution to regular ordering surrounded by smaller tubes. The large and small nanotube structure depended on the Zr content.
3. As Zr content increased, nanotube length of Ti-25Ta-xZr alloys increased.
4. As Zr content increased, HA precipitates changed leaf-like shape to rose-like shape.
5. RF-sputtered HA coating surface on HA deposited nanotubular Ti-25Ta-xZr alloys were covered entirely with the HA film. From the EDS results, Ti, Ta, Zr, Ca, P were detected in the coated layer.
6. Wettability increased in the order of bulk < nanotubular surface < HA coated nanotubular surface.

In conclusion, It is clear that HA coating on the nanotubular Ti-25Ta-xZr alloys have arrays of nano-HA structure. Also, RF-sputtered HA coating on HA deposited surface was densely coated HA precipitation compared to only HA coated surface. Therefore, surface morphology of nano-HA structure by electrochemical and physical vapor deposition will enhance osseointegration,

cell adhesion and bond strength.

- Reference -

1. H.C. Choe, W.G. Kim, Y.H. Jeong, *Surf. Coat. Technol.* 205 (2010) S305.
2. M.A. Khan, R.L. Williams, D.F. Williams, *Biomaterials* 20 (1999) 631.
3. M. Niinomi, *J. Mech. Behav. Biomed. Mater.* 1 (2008) 30.
4. Y.H. Jeong, H.C. Choe, W.A. Brantley, *Appl. Surf. Sci.* 258 (2012) 2129.
5. Y.L. Zhou, M. Niinomi, *Mater. Sci. Eng. C* 29 (2009) 1061.
6. J.A. Davidson, P. Kovacks, U.S. Patent no. 5, 169, 597, December 8, 1992.
7. W.G. Kim, H.C. Choe, *Thin Solid Films* 519 (2011) 7045.
8. T.J. Webster, C. Ergun, R.H. Doremus, R.W. Siegel, R. Bizios, *Biomaterials* 21 (2000) 1803.
9. J.M. Macak, H. Tsuchiya, A. Ghicov, K. Yasuda, R. Hahn, S. Bauer, P. Schmuki, *Curr. Opin. Solid State Mater. Sci.* 11 (2007) 3.
10. H.C. Choe, W.G. Kim, Y.H. Jeong, *Surf. Coat. Technol.* 205 (2010) S305.
11. Y.H. Jeong, W.G. Kim, G.H. Park, H.C. Choe, Y.M. Ko, *Trans. Nonferrous Met. Soc. China* 19 (2009) 852.
12. K.S. Raja, M. Misra, K. Paramguru, *Mater. Lett.* 59 (2005) 2141.
13. S.K. Yen, C.M. Lin, *Mater. Chem. Phys.* 77 (2002) 70.
14. Q. Zhang, Y. Leng, R. Xin, *Biomaterials* 26 (2005) 2865.
15. H.B. Hu, C.J. Lin, R. Hu, Y. Leng, *Mater. Sci. Eng. C* 20 (2002) 209.
16. W. Yue-qin, T. Jie, W. Ling, H. Ping-ting, W. Tao, *Trans. Nonferrous Met. Soc. China* 18 (2008) 631.
17. S. Ban, J. Hasegawa, *Biomaterials* 23 (2002) 2965.
18. K.V. Dijk, H.G. Schaeken, J.G.C. Wolke, J.A. Jansen, *Biomaterials* 17 (1996) 405.
19. R.G. Hennig, D.R. Trinkle, J. Bouchet, S.G. Srinivasan, R.C. Albers and J.W. Wilkins, *Nature Materials* 2 (2005) 129.
20. D. Salmon, *Low Temperature Data Handbook, Ti and Ti Alloys*, 1979.
21. R. Wood, *Ti Alloys Handbook, Metals and Ceramics Information Center, Battelle*, 1972, Publication number MCIC-HB-02.
22. J. Destefani, *ASM Handbook, vol. 2, ASM International* (1990) 586.

23. T.R. Rautray, R.Narayanan, K.H. Kim, *Prog. Mater. Sci.* 56 (2011) 1137.
24. K. Seshan, *Handbook of Thin-Film Deposition Processes and Techniques* 2nd Edition, 2002.
25. A.W. Tan, Pingguan-Murphy, R. Ahmad, S.A. Akbar, *Ceram. Int.* 38 (2012) 4421
26. G. Liu, K. Wang, N. Hoivik, H. Jakobsen, *Solar Energy Materials & Solar Cells* 98 (2012) 24.
27. G.K. Mor, O.K. Varghese, M. Paulose, K. Shankar, C.A. Grimes, *Solar Energy Materials & Solar Cells* 90 (2006) 2011.
28. S. Shadanbaz, G.J. Dias, *Acta biomaterialia* 8 (1012) 20.
29. A. Arifin, A.B. Sulong, N. Muhamad, J. Syarif, M.I. Ramli, *materials & design* 55 (2014) 165
30. T. Hanawa, *Jpn. Dent. Sci. Rev.* 46 (2010) 93.
31. FCM Driessens, *Monographs in oral science* 10 Karger, 1982.
32. H. Wender, P. Migowski, A.F. Feil, S.R. Teixeira, J. Dupont, *Coord. Chem. Rev.* 257 (2013) 2468.
33. Y.L. Zhou, M. Niinomi, T. Akahori, *Mater. Sci. Eng. A* 371 (2004) 283.
34. M. Abdel-Hady, H. Fuwa, K. Hinoshita, H. Kimura, Y. Shinzato, M. Morinaga, *Scr. Mater.* 57 (2007) 1000.
35. A.V. Dobromyslove, V.A. Elkin, *Scripta Mater.* 44 (2001) 905.
36. E.J. Kim, W.G. Kim, Y.H. Jeong, H.C. Choe, *J. Nanosci. Nanotechnol.* 11 (2011) 7433.
37. W.G. Kim, H.C. Choe, Y.M. Ko, W.A. Brantley, *Thin Solid Films* 517 (2009) 5033.
38. S.H. Jang, H.C. Choe, Y.M. Ko, W.A. Brantley, *Thin Solid Films* 517 (2009) 5038.
39. H.W. Kim, Y.H. Koh, L.H. Li, S. Lee, H.E. Kim, *Biomaterials* 25 (2004) 2533.
40. J.U. Kim, Y.H. Jeong, H.C. Choe, *Thin Solid Films* 520 (2011) 793.

감사의 글

어느덧 2년이 지나고 대학원생활을 졸업논문과 함께 마무리 하려고하니 지난 대학원 생활이 주마등처럼 지나갑니다. 그동안 연구실에서 함께 도와가며 보낸 시간들은 평생 잊지 못할 것 이며, 힘들 때마다 다시 회상하며 힘을 얻을 것 같습니다. 2년간의 석사생활을 마무리하며 석사과정을 무사히 보낼 수 있게 도움을 주신 분들께 짧게나마 감사의 마음을 전하려고 합니다.

우선 부족하지만 항상 다독여 주시고, 아낌없는 격려와 지도를 주신 평생 스승이신 지도교수 최한철 교수님의 은혜에 고개 숙여 감사드립니다. 또한 바쁘신 가운데도 꼼꼼하게 논문 심사 해주신 김병훈 교수님, 안상건 교수님에게도 감사드립니다. 교수님들 항상 건강하시고 좋은 일들만 가득하길 기원하겠습니다.

그리고 많은 조언과 관심 가져주신 용훈이형, 강이형, 병학이형, 영진이형, 재운이형, 은주 및 치과재료학교실 선배님들, 항상 고맙게 생각하고 있습니다. 그리고 친한 친구이자 동기 성환이, 우리가 알게 된지도 꽤 오래됐네. 포항 가서도 잘 할 거라 믿는다. 많이 챙겨주지 못했지만, 은실아 열심히 한 만큼 좋은 곳에서 좋은 결과 있길 바란다. 항상 옆에서 웃어주며 굶은일도 마다 않는 채익아, 실험실장으로서 치과재료학교실 잘 이끌어 갈 거라고 믿는다. 그리고 이번학기에 들어와서 누구보다 열심히 하는 인섭이 김정재 박사님, 많이 도움은 못줬지만 치과재료학교실 누구보다 잘 이끌어 갈 것 이라고 믿어 의심치 않습니다.

마지막으로 부족하지만 우리아들 최고라며 끝까지 믿고 응원해주신, 존재만으로도 큰 힘이 되는 부모님, 제가 열심히 할 수 있었던 이유이자 원동력이었습니다. 또한 힘들 때마다 큰 힘이 되어주고 웃을수 있게 해준 우리 누나 항상 고마워하는 거 알지. 앞으로 더욱더 열심히 하여 자랑스런 아들, 동생이 되도록 노력하겠습니다.

2014. 02.
김현주 올림

저작물 이용 허락서

학 과	광기술공학과	학 번	20127166	과 정	석사
성 명	한글: 김 현 주 한문 : 金 炫 柱 영문 : Hyun-Ju Kim				
주 소	광주광역시 북구 신안동 삼익@ 1동 1402호				
연락처	E-MAIL : dkldhr86@hanmail.net				
논문제목	한글 : 나노튜브 형성된 Ti-25Ta-xZr 합금에 전기화학적인 석출 후, RF-Sputtering을 이용한 HA코팅 영어 : Hydroxyapatite Coating on Nanotubular Ti-25Ta-xZr Alloys by RF-Sputtering after Electrochemical Deposition for Biomaterials				

본인이 저작한 위의 저작물에 대하여 다음과 같은 조건아래 조선대학교가 저작물을 이용할 수 있도록 허락하고 동의합니다.

- 다 음 -

1. 저작물의 DB구축 및 인터넷을 포함한 정보통신망에의 공개를 위한 저작물의 복제, 기억장치에의 저장, 전송 등을 허락함
2. 위의 목적을 위하여 필요한 범위 내에서의 편집·형식상의 변경을 허락함. 다만, 저작물의 내용변경은 금지함.
3. 배포·전송된 저작물의 영리적 목적을 위한 복제, 저장, 전송 등은 금지함.
4. 저작물에 대한 이용기간은 5년으로 하고, 기간종료 3개월 이내에 별도의 의사 표시가 없을 경우에는 저작물의 이용기간을 계속 연장함.
5. 해당 저작물의 저작권을 타인에게 양도하거나 또는 출판을 허락을 하였을 경우에는 1개월 이내에 대학에 이를 통보함.
6. 조선대학교는 저작물의 이용허락 이후 해당 저작물로 인하여 발생하는 타인에 의한 권리 침해에 대하여 일체의 법적 책임을 지지 않음
7. 소속대학의 협정기관에 저작물의 제공 및 인터넷 등 정보통신망을 이용한 저작물의 전송·출력을 허락함.

동의여부 : 동의(0) 반대()

2014 년 02 월 25 일

저작자: 김 현 주 (서명 또는 인)

조선대학교 총장 귀하